materials

MDPI

Article

Microwave Sintering of Alumina at 915 MHz: Modeling, Process Control, and Microstructure Distribution

Sylvain Marinel [1,*], Charles Manière [1], Anthony Bilot [1], Christelle Bilot [1], Christelle Harnois [1], Guillaume Riquet [1], François Valdivieso [2], Christophe Meunier [2], Christophe Coureau [3] and François Barthélemy [4]

1 Normandie Univ, ENSICAEN, UNICAEN, CNRS, CRISMAT, 14000 Caen, France
2 Laboratoire Georges Friedel, École des Mines de Saint-Étienne, 42023 Saint-Etienne, France
3 SOLCERA, ZI n 1 Rue de l'industrie, 27000 Evreux, France
4 DGA (Direction Générale de l'Armement), Echangeur de Guerry, 18000 Bourges, France
* Correspondence: sylvain.marinel@ensicaen.fr; Tel.: +33-(0)231-45-13-69

Received: 3 July 2019; Accepted: 7 August 2019; Published: 9 August 2019

Abstract: Microwave energy can be advantageously used for materials processing as it provides high heating rates and homogeneous temperature field distribution. These features are partly due to the large microwave penetration depth into dielectric materials which is, at room temperature, a few centimeters in most dielectric materials. However, up to now, this technology is not widely spread for high-temperature material processing applications (>1200 °C), because its reproducibly and ability to sinter large size samples (>30 cm^3) still needs to be improved. In this context, this paper describes both an empirically designed 915 MHz single-mode cavity made from SiC susceptors and refractory thermal insulation, and the 3D modeling of the process in order to improve our understanding of it. Different susceptors geometries and coupling slit position were numerically tested in order to better understand how these parameters impact the field homogeneity and the process stability. It was found that positioning the largest surface of the susceptors parallel to the electrical field allows a very uniform and hybrid heating of the material, while avoiding plasma or thermal instabilities. This was correlated to the 3D modeling results. Finally, thanks to a fully-automatized system this apparatus was used to sinter large size (~30 cm^3) low-loss dielectric alumina samples. The sintered materials were subsequently characterized in terms of density, grain size distribution, and homogeneity. The reproducibility was also discussed, demonstrating the process efficiency and reliability.

Keywords: microwave sintering; resonant applicator; process control; alumina; hybrid heating; modeling

1. Introduction

Microwave processing of materials is an emerging technology very appropriate for the synthesis or sintering of materials [1]. Recently, Kitchen et al. have reported different results related to the microwave synthesis of various types of materials, including oxides, carbides, or nitrides [2]. In a more detailed way, Croquesel et al. have presented specific instrumentation on a 2.45 GHz single-mode cavity for sintering alumina [3]. In terms of microwave–material interactions, Mishra and Sharma have discussed in detail how ceramic materials are heated by microwaves depending on their physical properties [4]. In the same way, Oghbaei and Mirzaee [5] have summarized the different advantages and challenges to face when microwave energy is used for the sintering of materials. The main advantages of microwave heating are the high heating rates and the volumetric heating thanks to the large penetration depth of the microwave radiation in dielectric materials (a few centimeters).

Therefore, the temperature field is expected to be homogeneous and the overall heating efficiency can be high. Even the flash microwave sintering process can be envisaged using direct microwave heating, as shown by Biesuz and Sglavo [6]. There are many experimental microwave systems for material sintering and most of them are designed by laboratories themselves; therefore, the heat treatment conditions cannot be easily compared from one experiment to another. For instance, for low-loss dielectric materials, such as alumina, spinel, or insulating perovskite, etc., researchers usually use susceptor materials to initiate the heating. These susceptors are made from highly microwave-absorbing materials such as silicon carbide, zirconia, etc. The effect of the susceptor material properties on the heating behavior was discussed by Heuguet et al. [7]. At low temperature, susceptors are directly heated by microwave and they allow the low-loss dielectric material to be heated mostly by thermal radiation. As the dielectric losses of the material increase with temperature, there is a critical temperature above which the sample starts to heat by itself. The latter process is called the hybrid heating process, as the heat is provided by both thermal heat flux coming from the susceptor and by direct conversion of the microwave energy in the material. Different types of susceptors can be found in the literature, including rod-like arrangement (picket–fence arrangement), powdered susceptors, or tubular susceptors. Bhattacharya et al. have described these different susceptor geometries [8]. Otherwise, these susceptors are often used in many different microwave applicators (single mode, rectangular, cylindrical, multimode, etc.) at different frequencies (5.8 GHz, 2.45 GHz, etc.). Most of the time, this is an empirical process that leads to the final geometry and assembly, based on considerations such as heating and temperature control; temperature distribution and rates, etc. In this work, our aim is to develop a fully-controlled microwave heating process to sinter low-loss dielectric refractory materials. For this purpose, a 915 MHz single-mode rectangular cavity was chosen, as it provides a high volume chamber and, compared to the common and widely spread 2.45 GHz frequency, the 915 MHz one offers a larger penetration depth, as discussed by Zhai [9]. In this work, an assembly consisting of a thermal insulation material, equipped with two SiC susceptor plates, was used to sinter large size alumina in a 915 MHz cavity. Our aim was to provide a hybrid heating process with very good temperature regulation and distribution. By doing so, a volumetric heating process is expected thanks to the well-established dielectric heating mechanism. Moreover, the use of susceptors also allows the sample not to be too rapidly cooled from its surface, and, as a result, a homogeneous temperature distribution can be obtained. Modeling results will also be advantageously used to improve our understanding of the overall process, and to clearly point out the strong effect of the assembly geometry to the heating behavior. A full automatization of the system will also be used, based on our previous development [10], to sinter low-dielectric-loss alumina materials. The microstructure of the materials being sintered will be fully characterized and discussed with respect to the experimental conditions. A reliable process leading to a reproducible microstructure will be researched. Overall, this paper presents the strategy and the different results obtained on hexagonal-shaped large alumina samples (>30 cm^3) fully sintered in our original rectangular microwave cavity.

2. Experimental

2.1. Experimental 915 MHz Equipment

Marinel et al. have previously described the 915 MHz microwave equipment [10]. Basically, the equipment consists of a 915 MHz source (GLP 50KSM, SAIREM, Neyron, France) which delivers a microwave power to a rectangular wave-guide. At the end of the microwave line, a single-mode applicator is used to heat up the material. The system is equipped with a 4 stubs automatic impedance plunger (AI4S from SAIREM, SAIREM, Neyron, France) and a motorized short-circuit piston/termination. Full automatization was implemented allowing a thermal cycle to be programmed (Figure 1).

The automatic system described elsewhere [10] mainly consists of using three internal and independent loops: One for maintaining the impedance matching, another one for keeping satisfactory

the resonance condition, and the last one for adjusting the incident microwave power through an auto-adaptive PID program (Proportional, Integral, Derivative). In order to tune the P, I, and D values required to calculate the incident power value (incident power feedback loop), an initial power of 700 W is systematically applied at the beginning of the cycle, and the response of the system is measured (i.e., the temperature). When the temperature achieves 460 °C, the power is automatically switched off and the cooling temperature is recorded. From the temperature response to the square signal, the P, I, and D coefficients initial values are calculated. Then the temperature regulation is automatically working by continuously adjusting the incident microwave power, calculated from the automatic calculated P, I, and D values. Therefore, the temperature signal can rigorously follow the programmed cycle.

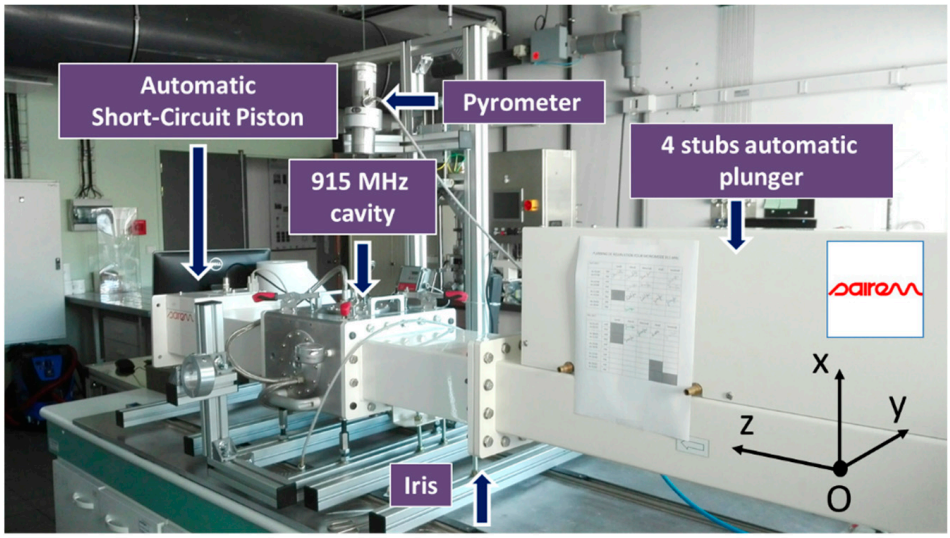

Figure 1. Photograph of the microwave system with the four-stub automatic impedance tuning device and the short-circuit piston.

2.2. Numerical Analysis

Understanding the previously described microwave system requires numerically solving a very complex multiphysics problem, where the microwave physics, resonance phenomena, and thermal dependence of material properties are key parameters, as described by Maniere et al. [11,12]. These parameters are coupled to each other, as the heating of the specimen and the tooling modifies the microwave properties, which in turn influence the cavity microwave distribution and the resonance performances. Maniere et al. have shown that the PID regulation system has to deal with the microwave cavity response to dimensional changes and with the temperatures change [13]. To show the interconnection between the microwave fields distribution, the heating, and the stability of the thermal distribution, a multiphysics simulation is necessary. This numerical tool is based on the finite element method (FEM). It encompasses the physics of microwaves through Maxwell's equations and the heat transfer through the heat equation and surface-to-surface thermal irradiation between the heating tool/specimen. This model combining the electromagnetism and the heat transfer equation was previously implemented by Maniere et al. [11]. Convection is another heat transfer mechanism which is classically simulated by fluid dynamic physics. Both Egorov studies [14,15] have already introduced the contribution of the convection phenomenon into their numerical model. However, due to the small distances between the susceptors and the specimen (few mm), the convection can be neglected here. Comsol Multiphysics is the FEM code used in this work. In this code, Maxwell's equations are combined to describe the microwave distribution using the following equation:

$$\nabla \times \left(\mu_r^{-1} \nabla \times \boldsymbol{E_r}\right) = k_0^2\left(\varepsilon_r - \frac{j\sigma}{\omega\,\varepsilon_0}\right)\boldsymbol{E_r} \quad (1)$$

with $\boldsymbol{E_r}$ defined by the harmonic electric field expression $\boldsymbol{E} = \boldsymbol{E_r} exp(j\omega t)$.

The heat transfer part of the electromagnetic-thermal model is governed by:

$$\rho C_p \frac{\partial T}{\partial t} + \nabla \cdot (-\kappa \nabla T) = Q_e \tag{2}$$

with dissipated microwave source term:

$$Q_e = \frac{1}{2}\left(\varepsilon_0 \varepsilon_r'' \boldsymbol{E}^2 + \mu_0 \mu_r'' \boldsymbol{H}^2\right) \tag{3}$$

The microwave boundary conditions are a rectangular TE10 port which simulates the microwave incident power and the absorption of the reflected power (role of the waveguide circulator in the experimental setup). The other external surfaces are assumed to be perfectly conductive, reflecting and confining the waves inside the cavity. The thermal problem is limited to the insulation box, the susceptor, and the specimen. The external insulation box boundary conditions are convection and radiation using:

$$\varphi_{csa} = h_{ia}(T_{air} - T) \tag{4}$$

$$\varphi_{rsa} = \sigma_s \epsilon \left({T_{air}}^4 - T^4\right) \tag{5}$$

with the coefficients values $h_{ia} = 5\ W m^{-2} K^{-1}$ and $\epsilon = 0.83$. The internal surface-to-surface thermal radiation is calculated considering each point emitted $e_b(T)$ and incoming radiation G. The relation between these quantities is defined through the radiosity J expression which is the total outgoing thermal radiative flux:

$$J = (1 - \epsilon)G + \epsilon e_b(T) = (1 - \epsilon)G + \epsilon n^2 \sigma_s T^4. \tag{6}$$

As this study focuses on the microwave heating, the sintering is not simulated. All the temperature-dependent properties used in the simulation are summarized in Appendix A, Table A1 [13] and Figure A1.

2.3. Materials Preparation and Characterization and the Microwave Assembly

Alumina from Baïkowski was selected (Al_2O_3, BMA15, 99.99%, D50 = 150 nm, 16 m^2/g) and large hexagonal-shaped samples were prepared by SOLCERA (Evreux, France) by slip casting (59 × 10 mm thickness, see Figure 2). A green density of 60% was obtained (theoretical density of alumina = 3.97 g/cm^3). Samples were conventionally sintered in air in our 915 MHz single-mode applicator. Samples were subsequently polished to a final step with colloidal silica suspension (STRUERS OP-U Non-Dry, Struers, Champigny sur Marne, France) and SEM microstructures were collected with ZEISS Supra 55 scanning electron microscope (ZEISS, Oberkochen, Germany). Density of materials was measured using Archimedes' method in ethanol and grain sizes were measured using the intercept method. Finally, the hardness was measured using Vickers indentation technique at 1 kgF for 15 s (CLEMEX MMT with digital camera, CLEMEX, Guimond Longueuil, Canada).

The microwave assembly designed for our purpose is shown in Figure 3. The alumina hexagonal sample was vertically placed onto an alumina support piece and the larger side of the sample was parallel to the z direction (see Figure 1). SiC plates (80 × 80 × 7 mm, Anderman Ceramics AC-RSiC-A, Recrystallized Silicon Carbide) were placed parallel to the sample in between, as schematically shown on Figure 3. This design was found to be optimal for homogenizing the temperature field within the material. Otherwise, as seen further, the modeling data will support this original geometry. A thermal insulation box was machined from an alumina silicate porous foam from RATH© and allowed the assembly to be thermally insulated. The TE 105 mode was tuned; therefore, the sample was located where the electrical field was maximum. A single-color pyrometer (IRCON modline 5G, Fluke Process Instruments, Roissy en France, France) with a temperature range of 350 °C < θ < 2000 °C was used for

measuring the temperature, targeting the upper side of the sample. Macaigne et al. [16] measured an apparent emissivity of ~0.7 at about 1500 °C on alumina. In this work, a similar apparent emissivity was found and this value was selected for all experiments. Practically, temperature calibration consists in measuring the "apparent emissivity" of the sample. For that, a piece of calibrating material was placed on a tiny hole in the sample surface and when the calibrating material starts melting, the emissivity of the IR pyrometer was tuned so that the measured temperature equals the calibrating material melting point (a Charged Coupled Device, CCD camera was used to observe the sample surface with the calibrating material). It was assumed that the calibrating material was at the same temperature (or very close) to the sample surface temperature. Nb_2O_5 oxide (melting point ~1512 °C) material was used as calibrating material. By doing so, an apparent emissivity of 0.7 was found; more details about this calibration can be found in [16].

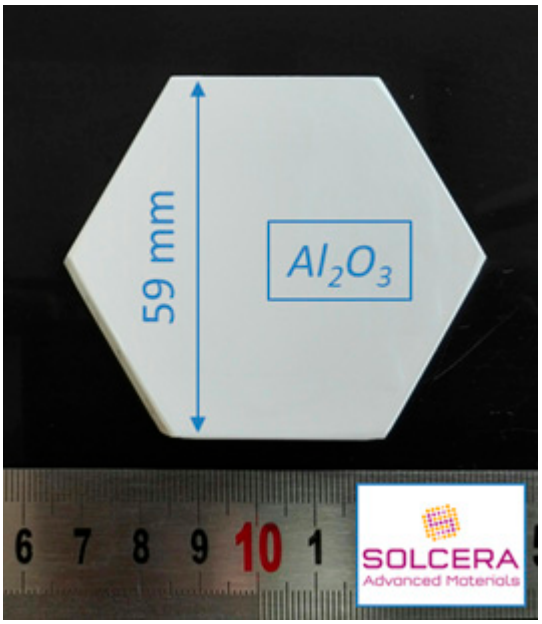

Figure 2. Picture showing a green sample of hexagonal-shaped alumina material. Samples were shaped by slip casting by SOLCERA Advanced Materials company.

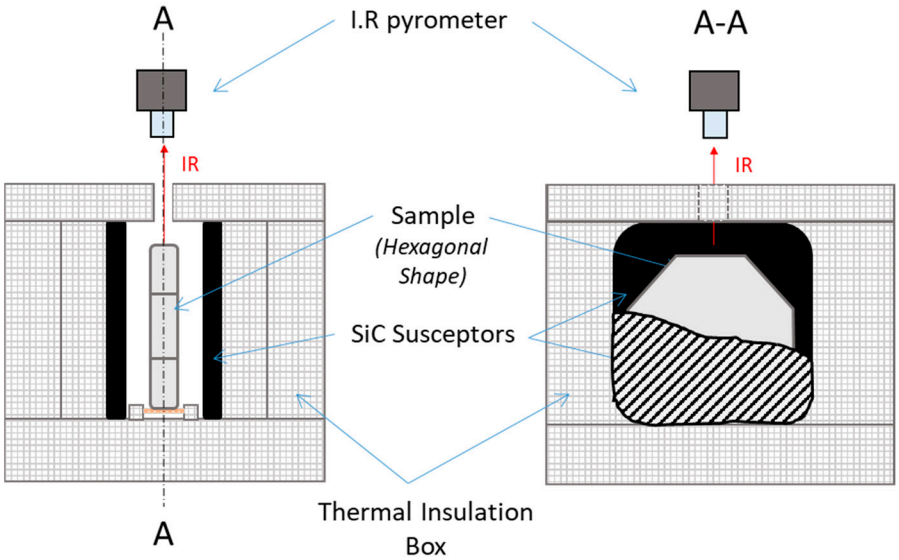

Figure 3. Assembly used to heat up the green ceramic sample into the 915 MHz single-mode cavity.

3. Results and Discussions

In this section, the microwave cavity is first presented through a simulation approach. The microwave distribution and heating are discussed. Then, the experimental results obtained for the hexagonal-shaped samples are presented and discussed with respect to simulation.

3.1. Microwave Cavity

The heating strategy of the 915 MHz cavity is first presented through pure microwave calculation. These steady-state parametric simulations consider a TE10 915 MHz microwave port, the iris, thermal insulation, SiC susceptors plates, and alumina hexagons. The main parameters are studied in order to explore this cavity potential, the orientation of the parallel SiC plates vs. E field, the distance between the iris and the specimen area, and, for each case, the total length of the cavity. The last parameter is essential as it allows the resonance (pseudo-resonance) phenomena to be located, which are highly sensible to the cavity dimensions at a given frequency. The microwave port parameter "S11", which quantifies the amount of reflected microwave (reflection coefficient) power, is used to locate the resonance phenomena, as it was previously described by Yakovlev et al. [17]. Resonance is associated with a minimal value of S11. In Figure 4 is presented the S11 curves, E field distribution for three SiC plate orientations and for two SiC properties. One corresponds to a SiC with high electrical conductivity (Batt et al.) and the other which is more classical (Baeraky see Figure A1). This shows clearly the strong influence of the susceptor orientation and properties with respect to the electrical field. If we consider the high-conductivity SiC (Figure 4a), when the susceptor plates are perpendicular to the electrical field, the coupling with microwaves is low and the resonant profile is very sharp, with, classically, a very high E field when close to the resonance. This abrupt resonant profile allows a high field intensity with a narrow resonance peak to be obtained. On the other hand, when the susceptor plates are oriented parallel to the electrical field, the resonant profile is nearly annihilated (highly conductive SiC), and this pseudo-resonant profile shows a very large peak with a small intensity shifted towards the lower cavity length value (peak position goes from ~485 mm down to ~440 mm). In this configuration, the high conductivity of SiC prevents a high resonant profile to develop in the cavity. In comparison, an important resonant profile is developed in the parallel configuration using the SiC properties of Baeraky, Figure 4b. The "parallel Y" configuration was used in previous work [10], and we see it corresponds to a configuration with SiC properties close to Baeraky's, which develops a high resonant profile. For the following simulation study, we will use Baeraky's properties.

In order to find the optimal position of the iris to locate the specimen in a maximal electrical field, another parametric study was investigated where the iris position and cavity length are explored. The results are reported in Figure 5. The iris position has an impact on the intensity and location of the pseudo-resonant profile. The optimal configuration in terms of position corresponds to the case where the iris is moved 40 mm closer to the specimen from initial position. In this position, the specimen is ideally located in the center of the waveguide electric field, while the internal electric field is high in the center of the specimen. This configuration is selected in the simulation of the microwave heating.

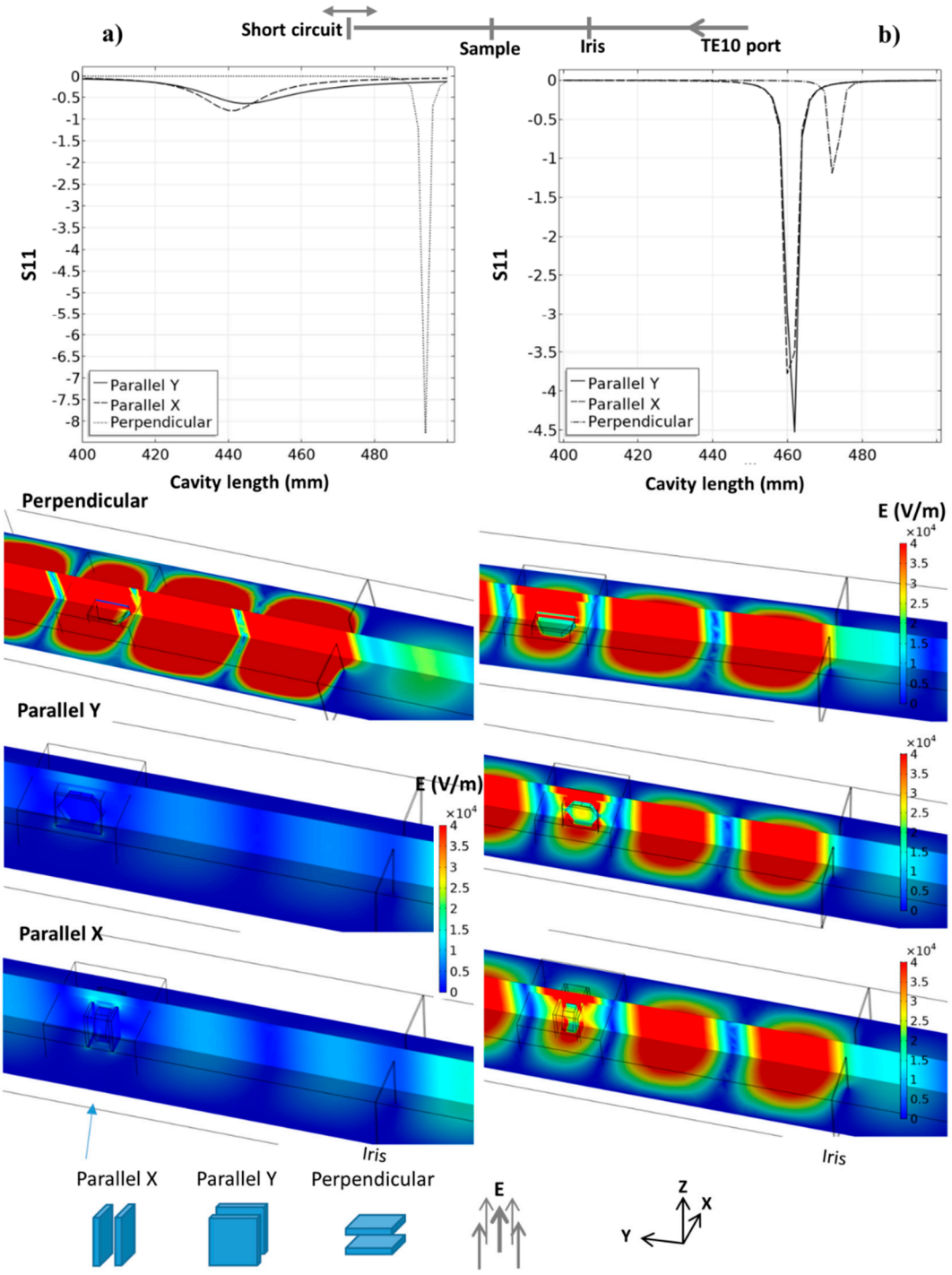

Figure 4. Resonant behavior of the 915 MHz cavity for three different orientations of the SiC susceptor plates with the E field; the simulation image corresponds to the minimum S11 parameter for each tested orientation; two SiC properties were used: (**a**) from Batt et al. and (**b**) from Baeraky, see Figure A1.

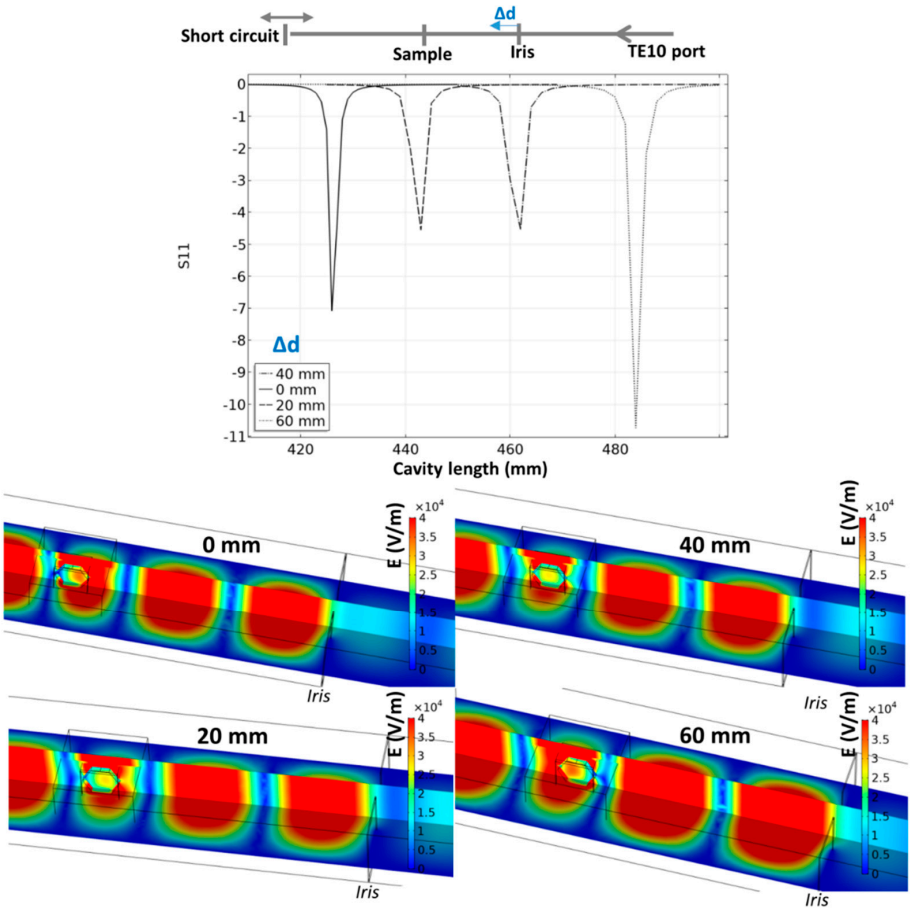

Figure 5. Resonant behavior of the 915 MHz cavity for different iris positions; the simulation images correspond to the minimum S11 parameter for each tested position.

3.2. Simulated Microwave Heating

The microwave heating is simulated in the "parallel Y" configuration (see Figure 4) with Baeraky SiC properties (see Figure A1) for a maximum microwave coupling of the SiC plates, and in an iris configuration where the electric field is centered on the sample ("40 mm configuration"; see Figure 5). The simulated temperature curves on the sample/susceptor and the thermal/electrical field during the heating, holding, and cooling are reported in Figure 6. The microwave incident powers were digitally PID regulated to impose the thermal cycle which will be used experimentally (see next section). The starting cavity length is in resonant configuration (configuration of Figure 5, 40 mm), as in reality an automatic PID adjusts the waveguide length via the automatic short-circuit. Because the heating of the alumina specimen is highly delayed compared to the susceptor (high thermal response), the PID-regulated temperature is the average temperature between the susceptor and the sample (see Figure 6). This way highly stabilizes the temperature regulation and is closer to the experimental conditions, whereby the thermal radiation coming from the susceptor participates in the apparent temperature measured by the pyrometer, which is pointed on the alumina sample upper surface, as discussed by Croquesel et al. [3]. As shown in Figure 6, the temperature difference between the susceptor and the sample is about 500 °C at the beginning, and this difference is decreasing down to a few degrees at 1000 °C. After this temperature, the temperature distribution is very homogeneous between the two susceptor plates. In Figure 6b, the microwave-dissipated heat is clearly active in the susceptor, while the alumina sample or the insulation contributes to about 5% of the relative part of the susceptor. The analysis of the heat flux (at high temperature Figure 6c) in the sample surface shows that the heat is transmitted to the sample mostly by thermal radiation from the susceptor to the sample. The dominant thermal exchange by radiation can be explained by the T^4 law (5). Because the alumina has a low dissipation factor compared

to the susceptor (SiC), the heating of the alumina hexagon is stabilized by the high external heat coming from the susceptor. Compared to the direct microwave heating, which is known to have high inherent heating instability (such as hot spots), the present study provides heating as stable as conventional sintering. Maniere et al. have clearly showed by modeling the advantage of using a hybrid configuration for stabilizing the thermal process [18]. Because the heating elements (susceptor) are closed to the specimen, faster heating cycles are allowed. It can be noted that, despite a low microwave–alumina coupling, a high electric field (2×10^4 V/m) is present in the sample volume. This high electric field may enhance the grain boundary diffusion, as suggested by Olevsky et al. [19]. This effect may accelerate the sintering kinetics under microwaves as proposed by Croquesel [3] and Olevsky et al. [19].

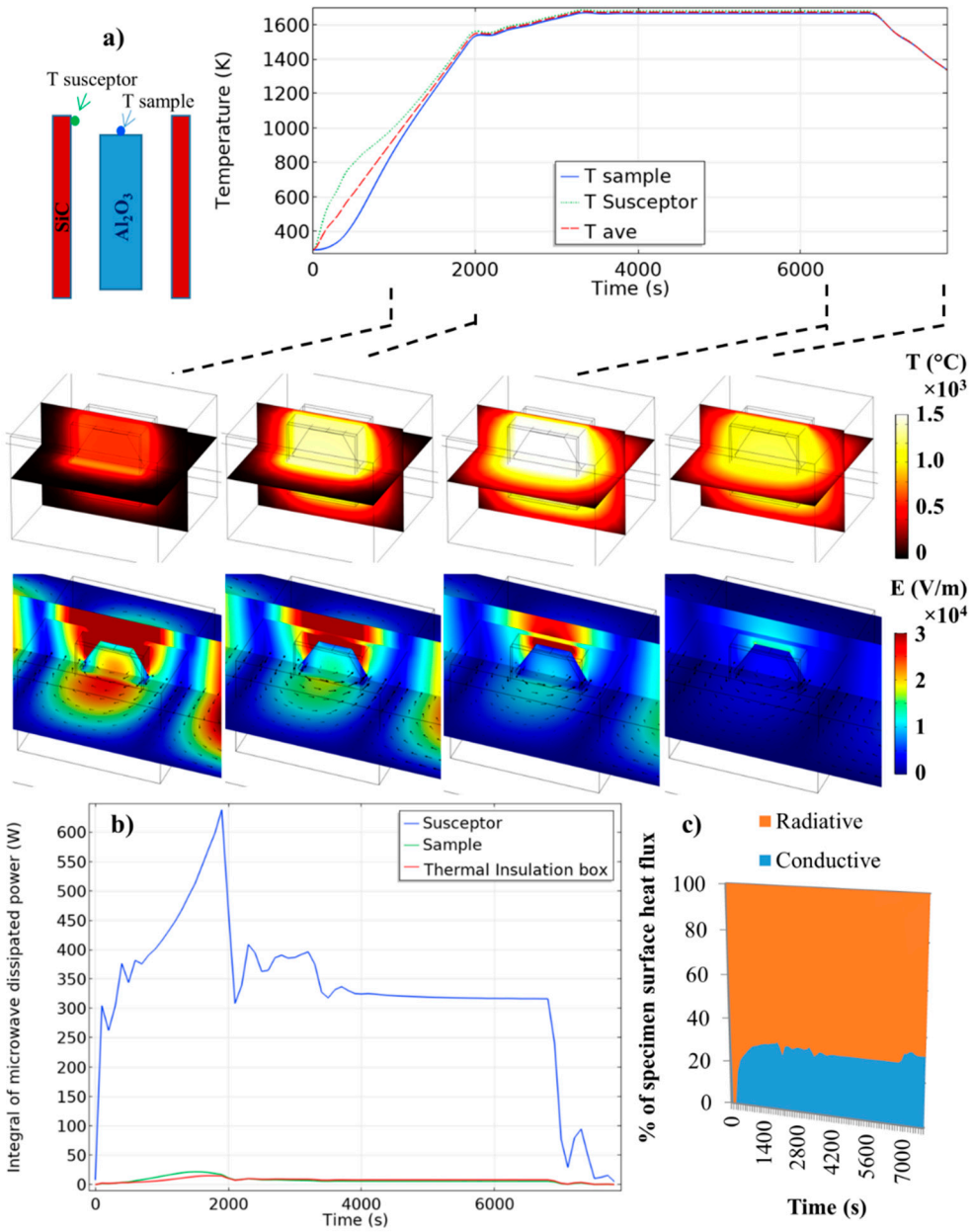

Figure 6. Electromagnetic-thermal simulation of the microwave-heated alumina specimen, (**a**) Temperature and electrical fields (black arrows are the magnetic field) and (**b**) dissipated thermal power in the insulation, sample, and susceptor, (**c**) percentage of the specimen surface heat flux (the convective flux is neglected due to the small air volume in the cavity).

3.3. Temperature Cycle and Sample Density

The geometry optimized by the simulation study was used to sinter hexagonal alumina samples in our 915 MHz cavity. The chosen temperature cycle is shown in Figure 7 and was defined from previous experiments on alumina. The PID auto adaptive process can be seen in this figure (see the red circle), where the temperature response to the 700 W imposed incident microwave power can be seen. Two heating ramps were programmed: One at 27 °C/min from RT to 1250 °C (1523 K to compare to modeling); and the second one at 7 °C/min, from 1250 to 1400 °C (1673 K). It was indeed necessary to slow down the heating ramp at high temperature, as the thermal losses (especially from thermal radiation) are very high at elevated temperatures. Therefore, the system could not follow the fastest imposed heating ramp (of 27 °C/min). The dwell temperature of 1400 °C (1673 K previously modeled) was found to be appropriate to get high density while avoiding significant grain growth. The sample density measured on the whole hexagonal sample is 99.6% of the theoretical value. The density was also measured on the six different triangles, previously cut from the hexagon. As shown in Figure 7 (see inset), it can be seen that the resulting density is similar from one location to another, showing that the sintering process is homogeneous. In order to check the reproducibility of the microwave heating system, several hexagons were sintered by using exactly the same conditions and thermal cycle. After sintering, all samples had the same density of ~99.6% of the theoretical value. As illustrated, Figure 8 shows an assembly of seven samples before and after sintering and clearly proves the good reproducibility of the as-developed microwave process.

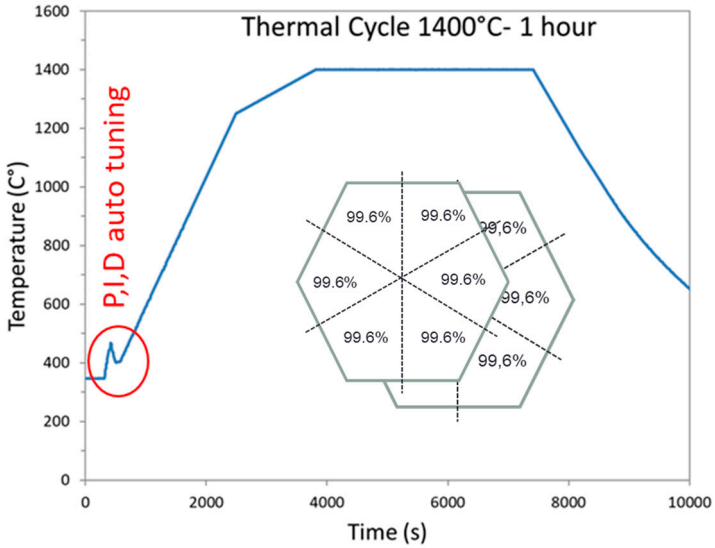

Figure 7. Heating program cycle imposed on sample during microwave sintering in our 915 MHz single-mode cavity.

Figure 9 shows the typical SEM microstructures of the alumina samples at different locations. First of all, the microstructures are dense and it can be clearly seen that the grain size is slightly smaller near the surface than in bulk. The grain size goes from around 1 μm at the sample surface to about 1.9 μm in the center. This shows that, despite the use of the SiC susceptors and its significant contribution in the heating process (see the modeling section), the center of the material does not densify with delay compared to its periphery. This is consistent with a hybrid heating mode, which results from the large microwave penetration depth into the material (at 915 MHz, 1400 °C, the penetration depth into alumina, calculated from the data Table A1, gives a value of 247 cm) and the quite high microwave electrical field (>2 kV/cm) which develops within the bulk alumina material, as estimated by modeling.

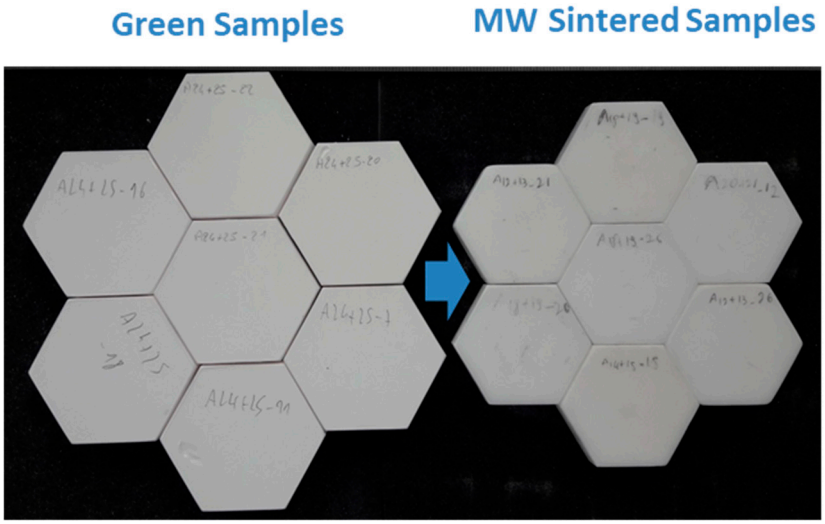

Figure 8. Several hexagon alumina samples microwave sintered.

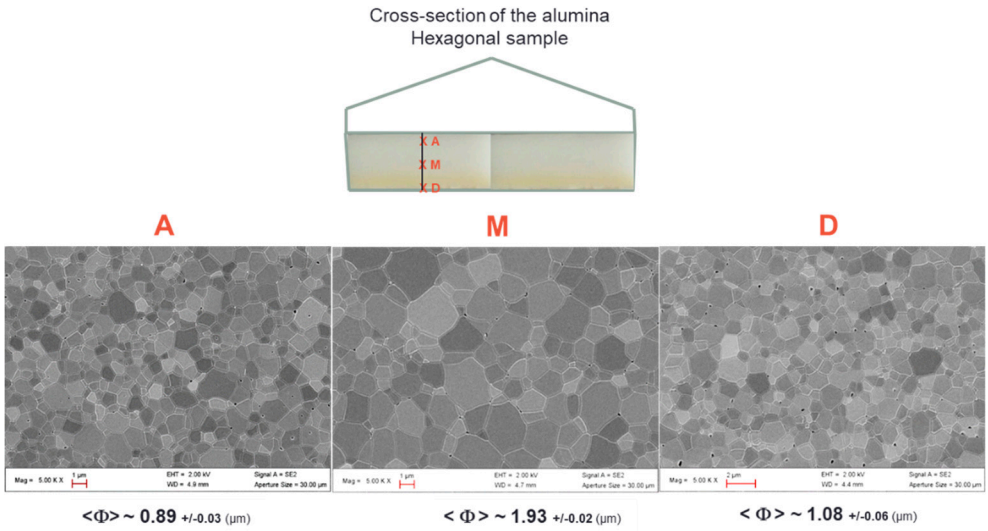

Figure 9. Typical SEM microstructures collected at the sample surface (A and D) and in the middle of the alumina hexagonal microwave sintered materials (M).

This grain size evolution is also reflected by the hardness value dependence on the position through the sample cross section (Figure 10). The hardness value is significantly higher in the sample periphery than in the bulk. An eye guide is plotted in red in the graph to ease the visualization of the hardness dependence with position. This hardness dependence is well correlated to the grain size distribution observed by SEM. Otherwise, the hardness value obtained is very close to the very high hardness value measured on submicronic grain size sintered samples by the spark plasma sintering process on the same alumina powder (up to HV1 ~21 GPa) [20].

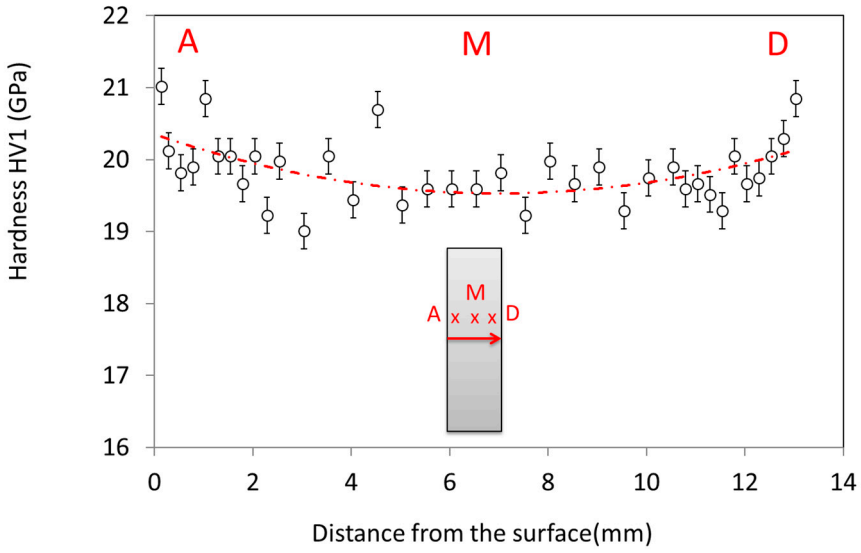

Figure 10. Plot of the hardness value as a function of the distance from the surface on a sample cross-section.

4. Conclusions

This work aimed at developing a fully automatized 915 MHz single-mode cavity to sinter large alumina samples. Modeling, temperature regulation, reproducibility of the process, and materials characterization were implemented and investigated. Through this research, an original susceptor SiC-plates assisted microwave process was designed in a rectangular 915 MHz microwave cavity. From the modeling results, it was shown that the most appropriate geometry was to align the largest surface of the SiC susceptors parallel to the electrical field. In the same way, the two susceptor plates were aligned along the microwave propagation direction. By doing so, a homogeneous heating of the sample with a very reliable temperature regulation process was achieved. Otherwise, this system was demonstrated to provide a hybrid heating mode, as shown by modeling. Experimentally, the grain size distribution revealed that grain size at the center is slightly larger than in the sample periphery, which could also be consistent with a hybrid heating mode. In terms of mechanical properties, the materials characterization reveals that highly dense materials (>99.6% dense) were produced exhibiting high hardness values (HV1~20 GPa). Finally, the as-developed process was found to be reproducible, clearly showing that these developments could bridge the gap in the use of microwave technology for high temperature sintering applications.

Author Contributions: Conceptualization, S.M., F.V. and C.C., modeling: C.M. (Charles Manière); methodology, A.B., C.M. (Christophe Meunier) and C.B., writing—original manuscript, S.M., writing—editing and reviewing, G.R. and C.H., funding acquisition, F.B.

Funding: The support of the Direction Générale de l'Armement (DGA) through the projects BAMBI (ref. ANR-11-ASTR-0025) and MAMBO (ref. ANR-16-ASMA-0003) is acknowledged.

Conflicts of Interest: The authors declare no conflicts of interest. The funders had no role in the design of the study; in the collection, analyses, or interpretation of data; in the writing of the manuscript, or in the decision to publish the results.

Nomenclature

ρ	Density (kg m^{-3})
C_p	Heat capacity (J·kg^{-1} K^{-1})
T	Temperature (K)
κ	Thermal conductivity (W m^{-1} K^{-1})
Q_e	Heat source (W m^{-3})
φ_{rsa}	Surface to ambient radiative heat flux (W m^{-2})

σ_s	Stefan Boltzmann constant (5.67×10^{-8} W m^{-2}·K^{-4})
ϵ	Emissivity
T_{air}	Air temperature (K)
φ_{csa}	Convective heat flux (W m^{-2})
h_{ia}	Surface conductivity (W m^{-2} K^{-1})
J	Surface radiosity (W m^{-2})
G	Irradiation flux (W m^{-2})
n	Refractive index
$e_b(T)$	Surface radiation produced (W m^{-2})
μ_r	Complex relative permeability
ε_r	Complex relative permittivity
μ_r''	Relative permeability imaginary part
ε_r''	Relative permittivity imaginary part
k_0	The vacuum wave number (rad·m^{-1})
σ	The electric conductivity (S·m^{-1})
ε_0	The vacuum permittivity ($8.854187817 \times 10^{-12}$ F m^{-1})
μ_0	The vacuum permeability ($1.2566370614 \times 10^{-6}$ T·m/A)
j	The complex number
ω	The angular frequency (rad Hz)
$\boldsymbol{E}$	Electric field strength (V m^{-1})
$\boldsymbol{H}$	The magnetic field intensity (A m^{-1})

Appendix A

Table A1. Electromagnetic-thermal properties of the insulating box and silicon carbide susceptor and alumina (T is temperature in K) [13].

Material	Symbol (Unit)	Temperature Range (K)	Expression
Insulation	Cp (J·kg^{-1}·K^{-1})	273–1600	$(-5.31 \times 10^{-4})T^2 + 1.25T + 5.18 \times 10^2$
	κ (W·m^{-1}·K^{-1})	273–1700	$1.70 \times 10^{-2} + (1.4\times 10^{-4})T$
	ρ (kg·m^{-3})	273–1700	$4.43 \times 10^2 - (1.04 \times 10^{-4})T$
SiC	Cp (J·kg^{-1}·K^{-1})	273–673	$-8.35 + 3.08T - 0.00293T^2 + (1.0268 \times 10^{-}6)T^3$
		673–1573	$772 + 0.431T - (2.10 \times 10^{-5})T^2$
		1573–1700	1400
	κ (W·m^{-1}·K^{-1})	273–1700	$192 - 0.326T + (2.74 \times 10^{-4})T^2 - (7.71 \times 10^{-8})T^3$
	ρ (kg·m^{-3})	273–1700	$2977 + 0.0510T - (2.29 \times 10^{-4})T^2 + (2.98 \times 10^{-7})T^3 - (1.92 \times 10^{-10})T^4 + (4.77 \times 10^{-14})T^5$
Al_2O_3	Cp (J·kg^{-1}·K^{-1})	273–1700	850
	κ (W·m^{-1}·K^{-1})	273–1700	$39{,}500T^{-1.26}$
	ρ (kg·m^{-3})	273–1700	3899
mAir	Cp (J·kg^{-1}·K^{-1})	273–1600	$0.177T + 961$
	κ (W·m^{-1}·K^{-1})	273–1600	$(6 \times 10^{-5})T + 0.0035$
	ρ (kg·m^{-3})	273–1700	$0.02897P/(RT)$
	Dynamic viscosity (Pa s)	273–1700	$2.82 \times 10^{-6} + (7.51 \times 10^{-8})T - (3.01 \times 10^{-11})T^2 + (8.88 \times 10^{-1})T^3 (-1.01 \times 10^{-18})T^4$
Insulation SiC Al_2O_3	Emissivity ϵ	273–1700	0.83 0.9 0.8
Insulation	ε_r'	273–1700	$(5.03 \times 10^{-8})T^2 + (1.37 \times 10^{-5})T + 1.5$
	ε_r''	273–1700	$(2.5 \times 10^{-9})T^2 - (1.64 \times 10^{-6})T + 3.96 \times 10^{-4}$
Al_2O_3	ε_r'	273–1700	$(1.34 \times 10^{-3})T + 8.3$
	ε_r''	273–1700	$(4.62 \times 10^{-5})T - 8.87 \times 10^{-3}$

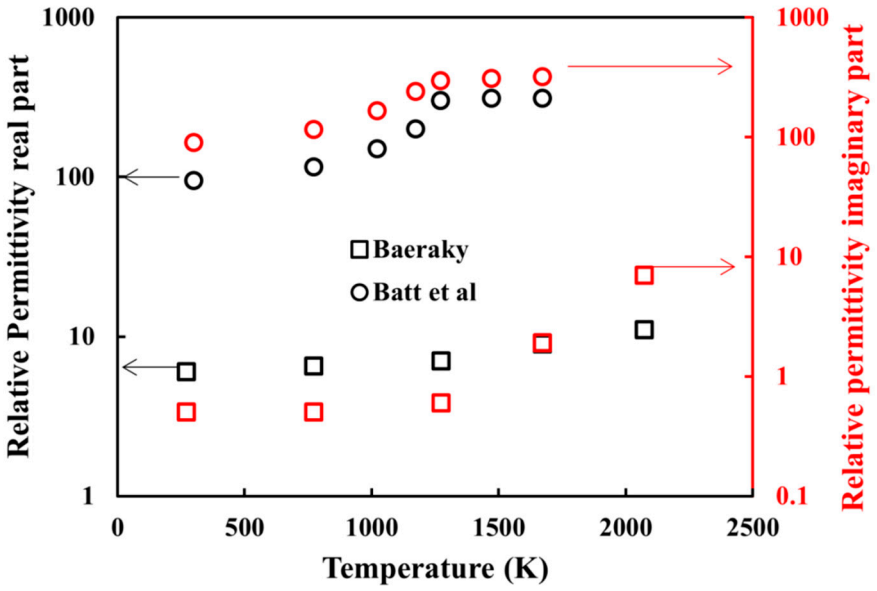

Figure A1. Complex relative permittivity of SiC from Baeraky [21] and Batt et al. [22].

References

1. Agrawal, D. Microwave sintering of ceramics, composites and metallic materials, and melting of glasses. *Trans. Indian Ceram. Soc.* **2006**, *65*, 129–144. [CrossRef]
2. Kitchen, H.J.; Vallance, S.R.; Kennedy, J.L.; Tapia-Ruiz, N.; Carassiti, L.; Harrison, A.; Whittaker, A.G.; Drysdale, T.D.; Kingman, S.W.; Gregory, D.H. Modern microwave methods in solid-state inorganic materials chemistry: From fundamentals to manufacturing. *Chem. Rev.* **2014**, *114*, 1170–1206. [CrossRef]
3. Croquesel, J.; Bouvard, D.; Chaix, J.; Carry, C.P.; Saunier, S. Development of an instrumented and automated single mode cavity for ceramic microwave sintering: Application to an alpha pure alumina powder. *Mater. & Des.* **2015**, *88*, 98–105. [CrossRef]
4. Mishra, R.R.; Sharma, A.K. Microwave–material interaction phenomena: Heating mechanisms, challenges and opportunities in material processing. *Compos. Part A: Appl. Sci. Manuf.* **2016**, *81*, 78–97. [CrossRef]
5. Oghbaei, M.; Mirzaee, O. Microwave versus conventional sintering: A review of fundamentals, advantages and applications. *J. Alloy. Compd.* **2010**, *494*, 175–189. [CrossRef]
6. Biesuz, M.; Sglavo, V.M. Flash sintering of ceramics. *J. Eur. Ceram. Soc.* **2019**, *39*, 115–143. [CrossRef]
7. Heuguet, R.; Marinel, S.; Thuault, A.; Badev, A. Effects of the susceptor dielectric properties on the microwave sintering of alumina. *J. Am. Ceram. Soc.* **2013**, *96*, 3728–3736. [CrossRef]
8. Bhattacharya, M.; Basak, T. A review on the susceptor assisted microwave processing of materials. *Energy* **2016**, *97*, 306–338. [CrossRef]
9. Zhai, D.; Wei, C.; Zhang, F.; Shang, X.; Chen, J.; Liu, M.; Peng, J. Microwave transmission performance of fused silica ceramics in microwave high-temperature heating. *Ceram. Int.* **2019**, *45*, 6157–6162. [CrossRef]
10. Marinel, S.; Renaut, N.; Savary, E.; Macaigne, R.; Riquet, G.; Coureau, C.; Gadeyne, T.; Guillet, D. Tuning, impedance matching, and temperature regulation during high-temperature microwave sintering of ceramics. *Adv. Mater. Sci. Eng.* **2018**. [CrossRef]
11. Manière, C.; Zahrah, T.; Olevsky, E.A. Fully coupled electromagnetic-thermal-mechanical comparative simulation of direct vs hybrid microwave sintering of 3Y-ZrO_2. *J. Am. Ceram. Soc.* **2017**, *100*, 2439–2450. [CrossRef]
12. Manière, C.; Chan, S.; Olevsky, E.A. Microwave sintering of complex shapes: From multiphysics simulation to improvements of process scalability. *J. Am. Ceram. Soc.* **2019**, *102*, 611–620. [CrossRef]
13. Manière, C.; Lee, G.; Zahrah, T.; Olevsky, E.A. Microwave flash sintering of metal powders: From experimental evidence to multiphysics simulation. *Acta Mater.* **2018**, *147*, 24–34. [CrossRef]
14. Manière, C.; Zahrah, T.; Olevsky, E.A. Fluid dynamics thermo-mechanical simulation of sintering: Uniformity of temperature and density distributions. *Appl. Therm. Eng.* **2017**, *123*, 603–613. [CrossRef]

15. Egorov, S.V.; Rybakov, K.I.; Semenov, V.E.; Bykov, Y.V.; Kanygina, O.N.; Kulumbaev, E.B.; Lelevkin, V.M. Role of convective heat removal and electromagnetic field structure in the microwave heating of materials. *J. Mater. Sci.* **2007**, *42*, 2097–2104. [CrossRef]
16. Macaigne, R.; Marinel, S.; Goeuriot, D.; Meunier, C.; Saunier, S.; Riquet, G. Microwave sintering of pure and TiO_2 doped $MgAl_2O_4$ ceramic using calibrated, contactless in-situ dilatometry. *Ceram. Int.* **2016**, *42*, 16997–17003. [CrossRef]
17. Yakovlev, V.; Allan, S.M.; Fall, M.L.; Shulman, H. Computational study of microwave processing of zirconia: Effects of frequency and temperature-dependent material parameters. In Proceedings of the 13th Seminar Computer Modeling in Microwave Engineering & Applications—Advances in Determining Material Parameters, Thun, Switzerland, 7–8 March 2011.
18. Manière, C.; Zahrah, T.; Olevsky, E.A. Inherent heating instability of direct microwave sintering process: Sample analysis for porous 3Y-ZrO_2. *Scr. Mater.* **2017**, *128*, 49–52. [CrossRef]
19. Olevsky, E.A.; Maximenko, A.L.; Grigoryev, E.G. Ponderomotive effects during contact formation in microwave sintering. *Model. Simul. Mater. Sci. Eng.* **2013**, *21*, 055022. [CrossRef]
20. Benaissa, S.; Hamidouche, M.; Kolli, M.; Fantozzi, G. Optical and mechanical characterization of transparent α-alumina fabricated by spark plasma sintering. *Int. J. Appl. Ceram. Technol.* **2019**, *16*, 638–646. [CrossRef]
21. Baeraky, T.A. Microwave measurements of the dielectric properties of silicon carbide at high temperature. *Egypt. J. Sol.* **2002**, *25*, 263–273.
22. Batt, J.; Sutton, W.H.; Binner, J.G.P.; Cross, T.E. *A Parallel Measurement Programme in High Temperature Dielectric Property Measurement: An Update*; American Ceramic Society: Westerville, OH, USA, 1995.

© 2019 by the authors. Licensee MDPI, Basel, Switzerland. This article is an open access article distributed under the terms and conditions of the Creative Commons Attribution (CC BY) license (http://creativecommons.org/licenses/by/4.0/).